A new dataset of soil Carbon and Nitrogen stocks and profiles from an instrumented Greenlandic fen designed to evaluate land-surface models

Xavier Morel[1], Birger Hansen[2], Christine Delire[1], Per Ambus[2], Mikhail Mastepanov[3,4], and Bertrand Decharme[1]

[1]CNRM UMR 3589, Meteo-France/CNRS, Toulouse, France
[2]Center for Permafrost (CENPERM), Department of Geosciences and Natural Resource Management, University of Copenhagen, Denmark
[3]Departement of Biosciences, Arctic Research Centre, Aarhus University, Roskilde, Denmark
[4]Oulanka research station, University of Oulu, Finland

Correspondence: Xavier Morel (morelxavier1@gmail.com)

Abstract. Arctic and boreal peatlands play a major role in the global carbon (C) cycle. They are particularly efficient at sequestering carbon because their high water content limits decomposition rates to levels below their net primary productivity. Their future in a climate-change context is quite uncertain in terms of carbon emissions and carbon sequestration.

Nuuk-fen is a well-instrumented greenlandic with monitoring of soil physical variables and greenhouse gas fluxes (CH_4
5 and CO_2) and is of particular interest for testing and validating land-surface models. But knowledge of soil carbon stocks and profiles is missing. This is a crucial shortcoming for a complete evaluation of models, as soil carbon is one of the primary drivers of CH_4 and CO_2 soil emissions. To address this issue, we measured for the first time soil carbon and nitrogen density, profiles and stocks in the Nuuk peatland (64°07,51"N , 51°23'10"W), colocated with the greenhouse gas measurements. Measurements were made along two transects, 60 and 90 m long and with a horizontal resolution of 5 meter and a vertical resolution of 5
10 to 10 cm, using a 4 cm diameter gouge auger. 135 soil samples were analyzed. Soil carbon density varied between 6.2 kg C m^{-3} to 160.2 with a mean value of 50.2 kg C m^{-3}. Mean soil nitrogen density was 2.37 kg N m^{-3}. Mean soil carbon and nitrogen stocks are 36.3 kg C m^{-2} and 1.7 kg N m^{-2}. These new data are in the range of those encountered in other arctic peatlands. This new dataset, one of very few in Greenland, can contribute to further development of joint modeling of greenhouse gas emissions and soil carbon and nitrogen in land-surface models. The dataset is open-access and available at
15 https://doi.org/10.1594/PANGAEA.909899.

1 Introduction

The terrestrial biosphere plays an important role in regulating atmospheric greenhouse gas composition and climate through gas exchanges and its capacity to act as a carbon (C) sink (Friedlingstein et al., 2019). For instance, northern latitude wetlands account for one third to one half of the methane emissions from natural wetlands (Schlesinger and Bernhardt, 2013). Among all terrestrial ecosystems, peatlands are arguably the most efficient at sequestering C over long time scales (Loisel et al., 2014; Leifeld and Menichetti, 2018). Peatlands are permanently saturated wetlands, and cover 3 % of the global land surface (Xu et al., 2018). In these ecosystems, the anaerobic conditions created by high water content lead to slow carbon decomposition. Because the accumulation rate of organic matter is greater than its decomposition rate, peatlands are important longterm soil carbon reservoir (Gorham, 1991). When undisturbed, these ecosystems are a net sink for atmospheric CO_2 (Jungkunst et al., 2012). Peatlands have consistently sequestering C although at variable rates throughout the entire Holocen period (Yu et al., 2011). Globally they are estimated to store between 550 and 694 GtC, about a third of global soil organic carbon stocks (Yu et al., 2010; Yu, 2012). Peatlands play a major role in the global carbon cycle (Harenda et al., 2018; Limpens et al., 2008).

Their future in a changing climate is quite uncertain, in terms of the magnitude of carbon emissions and sequestration (Yu et al., 2011). Recent projections suggest that peatlands may remain a carbon sink in the future, although a weaker one (Gallego-Sala et al., 2018). Primary productivity and soil carbon decomposition depend on multiple factors such as solar irradiance, air temperature, vegetation type, soil moisture, soil temperature, soil carbon and soil nutrient content, all of which depend on climate. To be able to estimate how much litter and soil carbon might be decomposed, it is necessary to know the carbon stock at present time. It is also important to know its vertical profile in the soil because the decomposition rate and ratio of CH_4 to CO_2 production depend on depth through soil temperature and soil moisture vertical profiles.

Nitrogen (N) is a limiting factor for plant growth and microbial activity in northern soils (Vitousek and Howarth, 1991) and could play an important role in future northern land carbon storage (Kicklighter et al., 2019) and greenhouse gas emissions (Luan et al., 2019). Increased nitrous oxide release from northern soils with permafrost thaw have been reported (Elberling et al., 2010; Voigt et al., 2017). However, very little is known on nitrogen stocks in these soils.

Knowledge of carbon and nitrogen stocks and profiles is hence particularly important. In the last decades, a growing number of sites in the arctic and boreal regions were instrumented in order to measure the greenhouse gas emissions of these ecosystems, such as Abisko in Sweden (Jammet et al, 2017), Samoylov in Russia (Siewert et al, 2015, 2016) or Zackenberg in Greenland (Pirk et al. 2016, 2017) (see Table 1). Similarly, more and more measurements of soil carbon stocks and profiles are conducted every year. Unfortunately, although large scale soil carbon databases already exist (e.g the Harmonized World Soil Database (FAO et al., 2012) or the Northern Circumpolar Soil Carbon Database (Hugelius et al., 2013), very few sites have both greenhouse gas flux and soil carbon content measurements (see Table 1). This is a substantial shortcoming that needs to be addressed, as carbon profiles are one of the primary drivers of CO_2 and CH_4 production and emission (Raich and Schlesinger,

1992). Moreover, for the few sites for which soil carbon stocks and greenhouse gas fluxes are available, both are quite often not measured at the same location (sometimes more than a few kilometers apart). Due to fine-scale heterogeneity (vegetation, microtopography, etc), they may reflect completely different conditions (e.g. first datasets from Zackenberg site (Sigsgaard et al., 2007; Palmtag et al., 2015)). From a site-scale modeling point-of-view, it is therefore important to have greenhouse gas

5   flux data (e.g. CH_4 and CO_2) and state variable data (C stocks and profiles) available at the same locations.

There are many challenges to simultaneously modeling greenhouse gas emissions and soil carbon in land-surface models. For instance, Chadburn et al. (2017) noted that models that simulate realistic soil temperature and soil carbon currently produce unrealistically low methane fluxes. It appears therefore necessary to improve the coupling of biogeochemical and physical

10   processes of land-surface models. An example of recent attempts at this is the biogeochemical carbon and greenhouse gas emissions model presented in Morel et al. (2019a) and embedded in the land surface model Interaction Soil-Biosphere-Atmosphere (ISBA; Noilhan and Planton (1989)). Although the biogeochemical and physical part of this model has been validated on three distinct boreal and arctic sites, the lack of soil carbon data did not allow a complete evaluation of this model. Hence, we conducted a field experiment in a well-instrumented greenlandic peatland, Nuuk-fen, to collect soil carbon stocks and profiles data

15   at the location of the automatic chambers measuring CH_4 and CO_2 fluxes and along two transects.

There is very little data available on wetlands in Greenland in general and fens in particular due to logistical difficulties to reach them. Fen extent in Greenland was recently estimated using a combination of remote sensing data and ground measurements (Karami et al., 2018). They find the extent of fen to be 4461 km^2, about 1.4% of the ice-free area and 5% of the vegetated

20   area of Greenland. In terms of in-situ data, (Palmtag et al., 2015, 2018) sampled a few fens for soil carbon and nitrogen in the Zackenberg valley. Barthelmes et al. (2015) in their review only list a dozen published in-situ measurements of peat deposits (both active and inactive), fairly shallow (less than 1 m) for the active ones. Among those, only 2 deal with carbon fluxes or stocks (MacDonald et al., 2006; Horwath Burnham and Sletten, 2010), the others being mostly paleoecological and archeological studies. Except for (Palmtag et al., 2018), none include nitrogen data. Hence, a new dataset on carbon and nitrogen content

25   of a Greenland fen is important.

The aim of this paper is to present and validate this new dataset of soil carbon and nitrogen stocks and profiles from Nuuk-fen. In Section 2 we present the Kobbefjord site, in particular the fen's physical characteristics and specificities. We present in Section 3 the experimental protocol and the methods of the field and laboratory studies. Section 4 presents collected

30   data of soil bulk density, water content, soil carbon content, profiles and stocks, as well as nitrogen and carbon/nitrogen (C/N) weight ratios. Finally, we discuss the dataset robustness and possible uses. These soil carbon and nitrogen data will complement the existing dataset of greenhouse gas fluxes from the fen. The combined dataset will allow to evaluate the fluxes and stocks simulated by land-surface models in a completely consistent manner. The dataset is open-access and available at https://doi.org/10.1594/PANGAEA.909899 (Morel et al., 2019b).

2 Study Area

The studied fen (Nuuk-fen) is located within the Nuuk Ecological Research Station and is part of the Greenland Ecosystem Monitoring program, which provides detailed reports on an annual basis, dating back to 2007 (Nuuk Ecological Research Operations - NERO - Annual reports ; Tamstorf et al. (2008)). The Research Station is well-instrumented and participates in several research programs, studying the dynamics of organisms and biological processes, the physical characteristics of marine, coastal and terrestrial environments, and performing climate and hydrology monitoring as well. Related data are public and open access on the Greenland Ecosystem Monitoring database repository, to be found at http://data.g-e-m.dk/.

Nuuk Research station is located in the south west of Greenland, in Kobbefjord (64°07'N ; 51°21'W), approximately 20 km from Nuuk. It is not in the permafrost region (Geng et al., 2019). According to the classification of Glooschenko et al. (1993) of Arctic and Subarctic wetlands, Nuuk fen is in the Low Subarctic Wetland Region. The research station consists of a drainage basin of 32 km^2 situated at the head of a fjord. The local climate is sub-Arctic with mean annual temperature of -1.4°C and mean annual precipitation of 752 mm (1961-90). Despite cold winter temperatures, the fen never freezes at depth below $10 - 15$ cm. NERO annual reports (Tamstorf et al., 2008; Raundrup et al., 2010) show a significant variability in soil texture, soil moisture, vegetation and microtopography. The studied zone, the only fen of the fjord, is surrounded by high rocks (left-top panel of Figure 1). The fen is located between the fjord and the Bade So lake. Datings of the sedimentary layer of Bade So (Larsen et al., 2017) showed that the lake was under sea level until 8500 BP. Hence, the fen can not be older. The underlying geology of the parent material is bedrock composed of Archaean tonalitic to granodioritic gneiss, and Qorqût granite (Larsen et al., 2017).

The fen is instrumented with automatic chambers, an eddy flux tower and a regular automated weather station, particularly useful for land-surface models. Nuuk CO_2 and CH_4 automatic chamber flux measurements started in 2007 and are still ongoing. The chambers usually operate from mid-May to mid-October. Each year, the CH4 flux peaks in July/August with values around 6 mg CH_4.m^{-2}.h^{-1}, and declines to about half of the maximum in early September. Peak CO_2 fluxes happen end of July - early August, reach about -300 mg CO_2.m^{-2}.h^{-1}, and occur at the peak of the growing season when photosynthesis is a much larger flux than soil respiration. These fluxes are described in Pirk et al. (2017); Morel et al. (2019a).

The main water inputs to the fen are from snowmelt and runoff from adjacent hills and inflow from a nearby stream located at the southern border of the fen (bottom panel of Figure 1). One key factor of this site appears to be the snowmelt date, as snowmelt water runs through the fen, leading to saturated moisture conditions during the growing season. We show that the darker areas in the center roughly correspond to the wetter areas. In these zones, the vegetation is adapted to saturated conditions. This vegetation for instance, has a lower albedo than in the fen's outer area, thereby absorbing more solar radiations compensating the colder conditions. Figure 2 shows the different vegetation types encountered throughout the fen : green herbaceous species and mosses in the outer part and aquatic plants with aerenchymas and *Sphagnum* in the center of the fen.

Section 3.1 explains more precisely the differences in vegetation.

3 Material and Methods

All the measurements were made in July 2017 along two transects, shown in the bottom panel of Figure 1. Each transect was
5   sampled every 5 meters, thus defining the plots $T1-0$, $T1-5$, $T1-10$ and so on.

The first transect (T1) roughly follows a N-S axis. The automatic chambers are situated on either side of the transect between plots $T1-0$ and $T1-20$. The second transect (T2) starts at the last automatic chamber, at the 20 meter plot of the first transect, in the middle of the fen and goes through the fen in its larger axis. The soil temperature probes can be seen between plots
10   $T2-30$ and $T2-45$.

3.1 Fen physical characteristics

First, we measured the topography of the fen and the depth of the sediment layer that delimits organic and mineral soil horizons at every plot for both transects. The elevation was measured with a topographer rod. The depth of the organic-mineral interface (OMI) was measured with a rigid metallic probe. The probe was lowered into the ground until a strong resistance, characteristic
15   of mineral soils, was encountered.

The first transect clearly revealed an accumulation basin at the center of the fen: while the ground elevetation remained approximately constant, the OMI depth strongly increased between plots $T1-0$ and $T1-25$ (Figure 3). This depression is characteristic for peatlands formation, and contributes to organic material accumulation and burial in these ecosystems. Its
20   maximal depth, of approximately 1 meter, was situated at T1-25 , and roughly corresponds to the darker part of the fen surface (Figure 1) and standing water (Figures 3.a and 2.b). The OMI depth sharply increased in 15 meters, then stayed relatively stable. The plot $T1-40$ seemed to mark the end of the fen. In this intermediate area from $T1-40$ to $T1-60$, surface moisture conditions were much drier (Figure 2.d) and the vegetation did not consist of aquatic plants such as *Sphagnum* anymore. Green herbaceous and mosses became then predominant. $T1-40$ to $T1-60$ are characterized by a hummocky topography (little
25   mounds and depressions)that cannot be picked up by 5 meter resolution measurements. The plot $T1-65$ was located at the shore of the nearby water stream.

The second transect started at the 20 meter plot of the first transect ($T2-0 = T1-20$), in the middle of the fen. Until plot $T2-30$, the soil elevation and the OMI depth did not vary much. There was a peak in the OMI depth at $T2-45$, surrounded
30   by two small depressions, while the soil elevation decreased. The end of the transect matched with the boundary of the fen. Approaching this boundary, the soil elevation and the mineral layer both rose.

3.2 Soil sampling along the transects

Soil samples were taken every 5 m along the first transect from the plots $T1 - 0$ to $T1 - 35$, as we focused solely on the peat deposit. As the second transect fully lay in the peat deposit, soil samples were taken every 10 m for the whole transect, i.e. between the plots $T2 - 0$ and $T2 - 80$. Samplings were made using a manual gouge auger, with double spade grip and a cylindrical semi-open lower part of 1 m depth and 4 cm in diameter. The general target depth of sampling was to reach below the peat/mineral transition. Samples were then extracted along the full soil core at regular intervals : every 5 cm in the top 15 centimeters, every 10 cm below. Soil samples were individually stored in small sealed plastic bags just after extraction in order to limit oxygen exchanges and halt decomposition.

Ideally, soil samples should be stored at a 4°C temperature before being transferred to the lab. With no fridge on the site, we used an insulated cooler in order to control at best the samples' temperature. The maximum elapsed time between sample collection and their deposit at the laboratory was three days. Although the temperature control of the samples may not have been optimal, this short delay between sample collection and handling prevented any significant decomposition.

3.3 Soil sample handling and analysis

Soil samples ($n = 135$) were first analyzed at the Greenland Institute of Natural Resources, located in Nuuk. For each sample, volume and mass were carefully measured following the method of Chambers et al. (2010) by removing a known-volume sample of peat using a volumetric sampler, measuring it again with a 0.1 mm precision vernier, and weighing it in a crucible in order to determine the samples density ρ_{sample} (g.m^{-3}).

Despite a careful measurement and a method designed to limit sample compaction, we recognize that some uncertainties on the samples densities are difficult to quantify :

1. The act of measurement and the soil core extraction can compress the samples within the manual gouge auger, hence modifying their structure.

2. Extracting the samples from the water-saturated soil layers without loss of water is obviously challenging, hence modifying the sample total mass. This potential loss of water can also change the available space within the soil pores, making the sample potentially more sensitive to any compaction.

3. The almost liquid texture of the water-saturated samples made it difficult to measure the sample volume. For these water-saturated samples, we used known volumes vials for volume measurements instead of the 0.1 mm precision vernier.

Peat samples were then oven-dried at 80 °C for 48 hours until a constant weight was reached (Djukic et al., 2018). Figure 4 shows samples at different depths for the soil cores $T1 - 10$ and $T1 - 25$ after drying. The samples of the $T1 - 10$ soil

core present a well-marked color gradient indicating the different soil horizons. For example, the colour and texture of sample $10 - 60/65$ (taken at $60 - 65$ cm depth) of plot $T1 - 10$ is characteristic of a mineral soil and corresponds indeed to the OMI (Figure 3). On the contrary, the $T1 - 25$ soil core (in the center of the fen) did not have any significant gradient of color and texture, except for a mixed-appearance zone at $60 - 65$ cm depth. We show later that these differences in color could be mainly explained by soil carbon content.

After drying, we determined the mass fraction of water of each sample, f_{wet}. In order to estimate the carbon density within the soil, we need the soil bulk density, ρ_{bulk}, defined as the dry mass per unit of total volume (Boelter, 1969; Hossain et al., 2015). The observed bulk density ρ_{bulk}^{obs} was computed as :

$$\rho_{bulk}^{obs} = \rho_{sample}(1 - f_{wet}) \tag{1}$$

Dried peat samples were then sent to the Center for Permafrost (CENPERM - University of Copenhagen - Denmark) for further C and N analysis. Briefly, 10 mg portions of thoroughly mixed and finely ground sample material were weighed into tin combustion cups for Dumas combustion (1700 °C) on an elemental analyser (CE 1110, Thermo Electron, Milan). Peat standards (Elemental Microanalysis, Okehampton, UK) were included for elemental analyser mass calibration in order to obtain percentage of C and N content, f_C and f_N respectively.

Soil carbon density ρ_C ($gC.m_{soil}^{-3}$) was then computed as :

$$\rho_C = \rho_{sample} f_C (1 - f_{wet}) = \rho_{bulk} f_C \tag{2}$$

Similarly, soil nitrogen density ρ_N ($gN.m_{soil}^{-3}$) was computed as :

$$\rho_N = \rho_{sample} f_N (1 - f_{wet}) = \rho_{bulk} f_N \tag{3}$$

A total of $n = 135$ samples were collected along both transects ($n_1 = 65$ and $n_2 = 70$). For each of these samples, values of mass, volume, density, dry mass, bulk density, carbon and nitrogen content (%) and density (kg.m^{-3}), and carbon-nitrogen (C/N) weight ratios were measured and/or calculated. Figure 5 shows distribution histograms for all data, and descriptive statistics (mean, median, upper and lower deciles) are presented in Table 2.

Figure 6 presents soil profiles of bulk density, water mass fraction, carbon and nitrogen content and density along both transects. These soil profiles ($n = 17$) were averaged over depth for both transects (Figure 7). As the fen depth showed a substantial variability along the transects, resulting averaged profiles are noisy. For instance, samples extracted at 50 cm depth may be in a purely organic soil horizon or a quasi-mineral one depending on the fen area it was extracted from. Hence, mean soil profiles

do not necessarily reflect the vertical distribution of data with respect to the OMI.

To reduce the noise due to the OMI heterogeneity, we renormalized all the data with respect to the OMI. For a sample extracted at a depth z from a peat core with an OMI depth z_{OMI}, we define its normalized distance from OMI d_{OMI} (%) as :

$$d_{OMI} = \frac{z}{z_{OMI}} \times 100 \tag{4}$$

These normalized profiles are shown in the Figure 8.

For each peat core, total carbon stocks C_T ($kgC.m^{-2}$) were calculated by vertically integrating carbon density profiles using the trapezoidal rule :

$$C_T = \sum_j (z_{j+1} - z_j) \frac{\rho_{C,j+1} + \rho_{C_j}}{2} \tag{5}$$

with z_j the sample depth and ρ_{C_j} the soil carbon density, computed using equation (2).

Similarly, total nitrogen stocks N_T (kgN.m^{-2}) were computed as :

$$N_T = \sum_j (z_{j+1} - z_j) \frac{\rho_{N,j+1} + \rho_{N_j}}{2} \tag{6}$$

with ρ_{N_j} the soil carbon density, computed using equation (3).

Note that because of the difficulties setting the manual gouge auger substantially below the OMI, the maximum sampling depth varied between the different peat cores. Hence, the integration depth also varied between peat cores. However, the carbon content below this interface did not exceed 7 % except for two unusual samples (Figure 9) and we can consider that not taking into account the soil horizons below the OMI did not underestimate much the computed total C stocks. Similarly, nitrogen content below the OMI are much lower than in the organic horizons (Figure 8), and not taking them into account did not underestimate much the computed total N stocks.

3.4 Calculation of 95% confidence interval soil profile

The sampling mean most likely follows a normal distribution. Under this hypothesis, for a variable X, the standard error of the mean can be calculated as $\sigma_{\overline{X}}(z) = \frac{\sigma(z)}{\sqrt{N(z)}}$ with N(z) the number of samples collected at a depth (z) and $\sigma(z)$ the standard deviation over those samples. The confidence interval at 95% is defined as $I(z) = \overline{X}(z) \pm 1.96 \times \sigma_{\overline{X}}(z)$.

4 Results and discussion

4.1 Bulk Density

Variation in bulk density is attributable to the relative proportion of organic and inorganic soil particles, and is a reliable indicator of the mineral or organic nature of a soil. More than 50% of the samples have a bulk density below 0.187 g.m^{-3} (Figure 5), characteristic of organic-rich material. Samples with bulk density between 0.5 and 1 g.cm^{-3} correspond to mixed organic-mineral material (Loisel et al., 2014). The higher the bulk density, the higher the mineral content. Finally, the 10% remaining samples with bulk densities higher than 0.978 g.cm^{-3} (Table 2) correspond to the part of the soil with the highest mineral fraction, near or below the OMI, as most mineral soils have bulk densities between 1.0 and 2.0 $g.cm^{-3}$ (Rezanezhad et al., 2016).

Strong vertical gradients in bulk density could be seen throughout both transects (Figure 6.a). The measured OMI depth delimited well the transition between organic and mineral material, as expected.

Typical bulk density profiles in peatlands tend to show a gradual increase with depth (Quinton et al., 2000) : as peat decomposition reduces the proportion of large pores by breaking down plant debris into smaller fragments (Rezanezhad et al., 2016), it increases the mass of dry material per volume of peat. Normalized mean profiles of bulk density (Figure 8.b) clearly shows this abrupt transition from mixed organic-mineral material to pure mineral soil below the OMI.

4.2 Carbon mass percentage

Mass percentage of carbon reached 50 % (Figure 6.c), which is coherent with the data given in the review of Yu (2012) on northern peatlands carbon stocks.

As expected, concentration of soil organic carbon in the organic layer was much higher than in the mineral horizons. High carbon content in the depth of the first transect seemed to indicate a carbon burial in the natural accumulation basin. We also note that the limit between the soil horizons with high and low carbon content also follows the OMI. In particular, the drop of the sedimentary layer in the first transect is clearly visible, and the variations of the mineral layer of the second transect between $T2-30$ and $T2-60$ meters as well. Normalized mean carbon content profiles (Figure 8.e) clearly showed the abrupt decrease in carbon content near the OMI. Below the OMI, carbon content values were below 10 %, which is coherent with the mineral characteristics of the soil horizons below.

4.3 Soil carbon density and soil carbon profiles

More than 70% of the soil samples had soil carbon densities comprised between 20 and 80 $kgC.m^{-3}$ (Figure 5.f). Those values are coherent with those encountered in other arctic and boreal fen and peatlands (see Chadburn et al. (2017), Fig.5). Mean local maximum of soil carbon density reached value up to $80kg.m^{-3}$ at 80 cm depth (Figure 7.f).

As expected, soil carbon density matched well the measured organic-mineral interface (Figure 6.e1). The assumed carbon accumulation in the accumulation basin of the fen discussed in the previous section is confirmed, as a local maximum of soil carbon density was clearly visible at the bottom of the soil plots $T1 - 25$ and $T2 - 30$ (Figure 6.a1).

5 Mean soil carbon density profiles were non-monotonous. In the organic horizons, SOC density increased with depth and reached its local maximum between 60 and 80 % of the organic-mineral interface depth (Figure 8.f). Near the OMI, coherent with the abrupt decrease in carbon content and increase in bulk density discussed in the previous sections, the soil carbon density decreased. Soil carbon density profiles that first increased and then decreased with depth are characteristic of arctic and boreal fens (see Chadburn et al. (2017), Fig.5).

10 **4.4 Integrated soil carbon stocks**

Tables 3 and 4 presents the carbon stocks and the maximum sampling depth for each peat core along both transects. Mean carbon stocks over both transects was 36.3 kgC.m^{-2}. The review of Yu (2012) on high-latitude fens and peatlands reports integrated soil carbon stocks values between 58.7 and 73.4 kgC.m^{-2}, except one extraordinary value of 113.6 kgC.m^{-2}. Those values are higher than those found in Nuuk. But they were computed by considering a fen depth of 1m, which was not the

15 case here, as the Nuuk fen is quite shallow: the mean sampling depth -which was often deeper than the OMI- did not exceed 76.3 cm in both transects (Tables 3 and 4). Hence, the results of our soil carbon stocks measurements were then coherent and consistent with current estimates from similar ecosystems.

Finally, a basic estimate of total soil carbon content over the whole fen area is given by multiplying the mean soil carbon mass per unit surface (36.3 kgC.m^{-2}) by a rough estimate of the fen area (approx. 7500 m2, see figure S2). This gives a total

20 carbon storage in the fen of 272 250 kgC.

4.5 Soil nitrogen density and soil nitrogen profiles

More than 70% of the soil samples had soil nitrogen densities between 1 and 4 $kgN.m^{-3}$ (Figure 5.h), with a mean value of 2.37 kgN.m^{-3}. The lowest values of N mass inicated the OMI (Figure 6.d). A local maximum of soil N density was clearly visible at the bottom of the soil plots $T1 - 25$ and $T2 - 20$ (Figure 6.a1), indicating that nutrients tend to accumulate in the fen

25 basin.

Soil N profiles follow closely the soil C profiles (Figure 7.f,h), indicating a quite uniform C/N ratio through the soil profile (see Section 4.7).

4.6 Integrated soil nitrogen stocks

Nitrogen stocks range from 0.8 kgN.m^{-2} and 2.9 kgN.m^{-2}, with a mean value of 1.7 kgN.m^{-2} (Tables 3 and 4). This is

30 very similar to the 1.9 ± 0.7 kgN.m^{-2} value obtained by Palmtag et al. (2018) (Table 2) for the fens on alluvial fans in the Zackenberg valley, to our knowledge the only available in-situ N data for Greenland peatlands. In a broader Arctic context,

these values are in the same range of terrestrial deposits in Alaskan Beaufort Sea Coast with 1.9 kgN.m^{-2} (0–100 cm; (Ping et al., 2011)) and slightly higher than an estimation for Arctic Alaska soils with 2.7 kgN.m^{-2} (0–100 cm: (Michaelson et al., 2013)).

5   A basic estimate of total soil nitrogen storage for the whole fen area is given by multiplying the mean soil nitrogen mass per unit surface (1.7 kgN.m-2) by a rough estimate of the fen area (approx. 7500 m2, see figure S2). This gives a total nitrogen storage in the fen of 12 882 kgN.

4.7 C/N Ratios

Carbon/nitrogen (C/N) weight ratios can give useful information about the nutrient content and the quality and humification
10 degree of organic matter : a low C/N ratio is usually equivalent to a high humification level. With a mean value of 21.6, observed C/N ratios were in the range of those observed from a variety of field and laboratory studies (Bridgham et al., 1998; Rezanezhad et al., 2016; Wang et al., 2015).

    C/N ratios were higher in the first few cm depth (approx. 25%), potentially indicating less microbial transformation of the
15 peat in the upper layers (Kuhry and Vitt, 1996). At greater depth of the fen, C/N ratios were lower because microorganisms slowly consume the carbon and recirculate the nitrogen, resulting in a gradual reduction of C/N values (Rydin and Jeglum, 2013). In northern regions, due to colder temperatures, the decomposition activity is slow, explaining the small difference between maximal and minimal C/N values. The C/N profiles remained relatively stable throughout the depth (21.6%) and the OMI did not seem to distinguish separate zones.
20 Although bulk density and C/N ratios are reliable indicator for peat degradation, the lack of ash content data and isotopic measurements did not allow a quantificiation of carbon accumuluation rate nor carbon loss in the peatland (Krüger et al., 2015).

4.8 Discussion

Overall, this new dataset of soil bulk density, carbon and nitrogen content, profiles and stocks from Nuuk-fen were in the range
25 of previous estimates of northern and arctics wetlands (Yu, 2012; Loisel et al., 2014; Chimner et al., 2014).

    As noted by Loisel et al. (2014), the accuracy of this type of measurement mostly depends on sample handling, in particular the care taken to avoid any peat compaction. Our sample density measurements may have been uncertain. On the other hand, mass carbon percentages are independent of any uncertainties or hazards in sample handling. It is known that soil carbon
30 content and bulk density are strongly correlated. For instance, Hossain et al. (2015) noted that bulk density ρ_{bulk}^{H} and carbon content f_C follow an exponential relationship :

$$\rho_{bulk}^{H} = ae^{-bf_C} \tag{7}$$

with $a = 1.5641$ and $b = 0.0631$.

We find a similar exponential behavior (figure 9.a) between bulk density and carbon content with a strong correlation between our measured bulk density and Hossein's exponential ($r^2 = 0.801$, Table 5). Different types of two-parameters regressions could also be used to infer bulk densities from carbon content, as shown in Table 5. Soil carbon density profiles can hence be computed with two different methods : a "direct" method, using bulk density data (see eq. 2), and an "indirect" method by computing bulk density using carbon content via one of these functional fits. This comparison shows that our measurements of bulk densities were in the right order of magnitude. But these relationships can not capture the vertical variability of the observed soil carbon profiles. Mass percentage of carbon f_C (%C) does not encapsulate all the causes of the variability of ρ_{bulk}. Consequently, inferred carbon profiles from indirect methods were deceptively flat and smooth (see Figure S1). Hence, although testing whether bulk density and soil carbon content measurements follow this type of relationship provides a good indicator of the dataset quality, it is not recommended to infer soil carbon profiles from these empirical relationships.

Loisel et al. (2014) choose an arbitrary cutoff value of 0.5 g.cm^{-3} to distinguish peat and non-peat material. It also roughly corresponds to the separation between samples with carbon content exceeding 15 % and the others (Figures 9.a,b,c). Below this threshold (i.e. for fully organic samples), there was a linear relationship between bulk density ρ_{bulk} and soil carbon density ρ_C (Figures 9.b), indicating a rather homogeneous soil carbon content f_C for organic samples. For mixed-material and mineral samples, such relationship is not true.

The well-known high water-retention capacity of peat soils (e.g. (Boelter, 1969)) was also observed here (Figure 9.c) as the higher values of soil-water content were found in the samples with the highest carbon content and lowest bulk density.

Finally, when using these data for performing a detailed 1-dimensional evaluation of the litter and soil carbon together with the $C0_2$ and CH_4 emissions simulated by a land-surface model, it is best to use the soil carbon data corresponding to the automatic chambers area, that is the profiles from plots $T1 - 0$ to $T1 - 20$.

5   Code and data availability

All the data used to produce the tables and figures of the paper are freely available on the repository :
https://doi.org/10.1594/PANGAEA.909899 (Morel et al., 2019b)

6   Conclusions and perspectives

In this paper, we have provided a complete description of a new dataset of the current distribution of soil organic carbon and nitrogen storage at the Nuuk peatland. This dataset is one of the very few on Greenland fens and will help in better understand-

ing these poorly documented ecosystems. All data are in the range of the existing arctic and low arctic fen studies. All data are in the range of previous studies. Automatic chamber flux measurements and carbon sampling are being recorded at the same location, making the Nuuk-fen dataset an ideal candidate for evaluating the accuracy of land surface model simulations of both soil carbon profiles and greenhouse gas emissions.

5 It will allow in the near future a complete evaluation of the biogeochemical model presented in Morel et al. (2019a). Completing this evaluation could help eventually resolve issues concerning biogeochemical models that model both soil carbon stocks/profiles and soil greenhouse gas fluxes raised by Chadburn et al. (2017). It could also be used to further validate recent devlopments in carbon and/or peatlands modules for larger scale studies, such as the specific peatland module developed by Largeron et al. (2018) or the soil carbon representation specific to fen and peatlands of Qiu et al. (2018).

References

Barthelmes, A., Couwenberg, J., Risager, M., Tegetmeyer, C., and Joosten, H.: Peatlands and Climate in a Ramsar context : A Nordic-Baltic Perspective, https://doi.org/10.6027/TN2015-544, 2015.

Boelter, D. H.: Physical Properties of Peats as Related to Degree of Decomposition1, Soil Science Society of America Journal, 33, 606, https://doi.org/10.2136/sssaj1969.03615995003300040033x, 1969.

Bridgham, S., Updegraff, K., and Pastor, J.: Carbon, Nitrogen, and Phosphorus Mineralization in Northern Wetlands, Ecology, 79, 1545–1561, https://doi.org/10.1890/0012-9658(1998)079[1545:CNAPMI]2.0.CO;2, 1998.

Chadburn, S. E., Krinner, G., Porada, P., Bartsch, A., Beer, C., Belelli Marchesini, L., Boike, J., Ekici, A., Elberling, B., Friborg, T., Hugelius, G., Johansson, M., Kuhry, P., Kutzbach, L., Langer, M., Lund, M., Parmentier, F.-J. W., Peng, S., Van Huissteden, K., Wang, T., Westermann, S., Zhu, D., and Burke, E. J.: Carbon stocks and fluxes in the high latitudes: using site-level data to evaluate Earth system models, Biogeosciences, 14, 5143–5169, https://doi.org/10.5194/bg-14-5143-2017, 2017.

Chambers, F., Beilman, D., and Yu, Z.: Methods for determining peat humification and for quantifying peat bulk density, organic matter and carbon content for palaeostudies of climate and peatland carbon dynamics, Mires and Peat, 7, 1–10, 2010.

Chimner, R. A., Ott, C. A., Perry, C. H., and Kolka, R. K.: Developing and Evaluating Rapid Field Methods to Estimate Peat Carbon, Wetlands, 34, 1241–1246, https://doi.org/10.1007/s13157-014-0574-6, 2014.

Djukic, I., Kepfer-Rojas, S., Schmidt, I. K., Larsen, K. S., Beier, C., Berg, B., Verheyen, K., Caliman, A., Paquette, A., Gutiérrez-Girón, A., Humber, A., Valdecantos, A., Petraglia, A., Alexander, H., Augustaitis, A., Saillard, A., Fernández, A. C. R., Sousa, A. I., Lillebø, A. I., [da Rocha Gripp], A., Francez, A.-J., Fischer, A., Bohner, A., Malyshev, A., Andrić, A., Smith, A., Stanisci, A., Seres, A., Schmidt, A., Avila, A., Probst, A., Ouin, A., Khuroo, A. A., Verstraeten, A., Palabral-Aguilera, A. N., Stefanski, A., Gaxiola, A., Muys, B., Bosman, B., Ahrends, B., Parker, B., Sattler, B., Yang, B., Juráni, B., Erschbamer, B., Ortiz, C. E. R., Christiansen, C. T., Adair], E. C., Meredieu, C., Mony, C., Nock, C. A., Chen, C.-L., Wang, C.-P., Baum, C., Rixen, C., Delire, C., Piscart, C., Andrews, C., Rebmann, C., Branquinho, C., Polyanskaya, D., Delgado, D. F., Wundram, D., Radeideh, D., Ordóñez-Regil, E., Crawford, E., Preda, E., Tropina, E., Groner, E., Lucot, E., Hornung, E., Gacia, E., Lévesque, E., Benedito, E., Davydov, E. A., Ampoorter, E., Bolzan, F. P., Varela, F., Kristöfel, F., Maestre, F. T., Maunoury-Danger, F., Hofhansl, F., Kitz, F., Sutter, F., Cuesta, F., [de Almeida Lobo], F., [de Souza], F. L., Berninger, F., Zehetner, F., Wohlfahrt, G., Vourlitis, G., Carreño-Rocabado, G., Arena, G., Pinha, G. D., González, G., Canut, G., Lee, H., Verbeeck, H., Auge, H., Pauli, H., Nacro, H. B., Bahamonde, H. A., Feldhaar, H., Jäger, H., Serrano, H. C., Verheyden, H., Bruelheide, H., Meesenburg, H., Jungkunst, H., Jactel, H., Shibata, H., Kurokawa, H., Rosas, H. L., Villalobos], H. L. R., Yesilonis, I., Melece, I., Halder], I. V., Quirós, I. G., Makelele, I., Senou, I., Fekete, I., Mihal, I., Ostonen, I., Borovská, J., Roales, J., Shoqeir, J., Lata, J.-C., Theurillat, J.-P., Probst, J.-L., Zimmerman, J., Vijayanathan, J., Tang, J., Thompson, J., Doležal, J., Sanchez-Cabeza, J.-A., Merlet, J., Henschel, J., Neirynck, J., Knops, J., Loehr, J., [von Oppen], J., Þorláksdóttir, J. S., Löffler, J., Cardoso-Mohedano, J.-G., Benito-Alonso, J.-L., Torezan, J. M., Morina, J. C., Jiménez, J. J., Quinde, J. D., Alatalo, J., Seeber, J., Stadler, J., Kriiska, K., Coulibaly, K., Fukuzawa, K., Szlavecz, K., Gerhátová, K., Lajtha, K., Käppeler, K., Jennings, K. A., Tielbörger, K., Hoshizaki, K., Green, K., Yé, L., Pazianoto, L. H. R., Dienstbach, L., Williams, L., Yahdjian, L., Brigham, L. M., [van den Brink], L., Rustad, L., Zhang, L., Morillas, L., Xiankai, L., Carneiro, L. S., Martino], L. D., Villar, L., Bader, M. Y., Morley, M., Lebouvier, M., Tomaselli, M., Sternberg, M., Schaub, M., Santos-Reis, M., Glushkova, M., Torres, M. G. A., Giroux, M.-A., [de Graaff], M.-A., Pons, M.-N., Bauters, M., Mazón, M., Frenzel, M., Didion, M., Wagner, M., Hamid, M., Lopes, M. L., Apple, M., Schädler, M., Weih, M., Gualmini, M., Vadeboncoeur, M. A., Bierbaumer, M., Danger, M., Liddell, M., Mirtl, M., Scherer-Lorenzen, M., Růžek, M., Carbognani, M., Musciano], M. D., Matsushita, M., Zhiyanski, M., Pușcaș, M., Barna, M.,

Ataka, M., Jiangming, M., Alsafran, M., Carnol, M., Barsoum, N., Tokuchi, N., Eisenhauer, N., Lecomte, N., Filippova, N., Hölzel, N., Ferlian, O., Romero, O., Pinto, O. B., Peri, P., Weber, P., Vittoz, P., Turtureanu, P. D., Fleischer, P., Macreadie, P., Haase, P., Reich, P., Petřík, P., Choler, P., Marmonier, P., Muriel, P., Ponette, Q., Guariento, R. D., Canessa, R., Kiese, R., Hewitt, R., Rønn, R., Adrian, R., Kanka, R., Weigel, R., Gatti, R. C., Martins, R. L., Georges, R., Meneses, R. I., Gavilán, R. G., Dasgupta, S., Wittlinger, S., Puijalon, S., Freda, S., Suzuki, S., Charles, S., Gogo, S., Drollinger, S., Mereu, S., Wipf, S., Trevathan-Tackett, S., Löfgren, S., Stoll, S., Trogisch, S., Hoeber, S., Seitz, S., Glatzel, S., Milton, S. J., Dousset, S., Mori, T., Sato, T., Ise, T., Hishi, T., Kenta, T., Nakaji, T., Michelan, T. S., Camboulive, T., Mozdzer, T. J., Scholten, T., Spiegelberger, T., Zechmeister, T., Kleinebecker, T., Hiura, T., Enoki, T., Ursu, T.-M., [di Cella], U. M., Hamer, U., Klaus, V. H., Rêgo, V. M., Cecco], V. D., Busch, V., Fontana, V., Piscová, V., Carbonell, V., Ochoa, V., Bretagnolle, V., Maire, V., Farjalla, V., Zhou, W., Luo, W., McDowell, W. H., Hu, Y., Utsumi, Y., Kominami, Y., Zaika, Y., Rozhkov, Y., Kotroczó, Z., and Tóth, Z.: Early stage litter decomposition across biomes, Science of The Total Environment, 628-629, 1369 – 1394, https://doi.org/https://doi.org/10.1016/j.scitotenv.2018.01.012, 2018.

Elberling, B., Christiansen, H., and Hansen, B.: High nitrous oxide production from thawing permafrost, Nature Geoscience, 3, https://doi.org/10.1038/ngeo893, 2010.

FAO, ISRIC, ISSCAS, and JRC: Harmonized World Soil Database (version 1.2). FAO, Rome, Italy and IIASA, Laxenburg, Austria, http://webarchive.iiasa.ac.at/Research/LUC/External-World-soil-database/HTML/, 2012.

Friedlingstein, P., Jones, M. W., O'Sullivan, M., Andrew, R. M., Hauck, J., Peters, G. P., Peters, W., Pongratz, J., Sitch, S., Le Quéré, C., Bakker, D. C. E., Canadell, J. G., Ciais, P., Jackson, R. B., Anthoni, P., Barbero, L., Bastos, A., Bastrikov, V., Becker, M., Bopp, L., Buitenhuis, E., Chandra, N., Chevallier, F., Chini, L. P., Currie, K. I., Feely, R. A., Gehlen, M., Gilfillan, D., Gkritzalis, T., Goll, D. S., Gruber, N., Gutekunst, S., Harris, I., Haverd, V., Houghton, R. A., Hurtt, G., Ilyina, T., Jain, A. K., Joetzjer, E., Kaplan, J. O., Kato, E., Klein Goldewijk, K., Korsbakken, J. I., Landschützer, P., Lauvset, S. K., Lefèvre, N., Lenton, A., Lienert, S., Lombardozzi, D., Marland, G., McGuire, P. C., Melton, J. R., Metzl, N., Munro, D. R., Nabel, J. E. M. S., Nakaoka, S.-I., Neill, C., Omar, A. M., Ono, T., Peregon, A., Pierrot, D., Poulter, B., Rehder, G., Resplandy, L., Robertson, E., Rödenbeck, C., Séférian, R., Schwinger, J., Smith, N., Tans, P. P., Tian, H., Tilbrook, B., Tubiello, F. N., van der Werf, G. R., Wiltshire, A. J., and Zaehle, S.: Global Carbon Budget 2019, Earth System Science Data, 11, 1783–1838, https://doi.org/10.5194/essd-11-1783-2019, 2019.

Gallego-Sala, A., Charman, D., Brewer, S., E. Page, S., Prentice, I., Friedlingstein, P., Moreton, S., J. Amesbury, M., W. Beilman, D., Björck, S., Blyakharchuk, T., Bochicchio, C., K. Booth, R., Bunbury, J., Camill, P., Carless, D., Chimner, R., Clifford, M., Cressey, E., and Zhao, Y.: Latitudinal limits to the predicted increase of the peatland carbon sink with warming, Nature Climate Change, 8, https://doi.org/10.1038/s41558-018-0271-1, 2018.

Geng, M. S., Christensen, J. H., and Christensen, T. R.: Potential future methane emission hot spots in Greenland, Environmental Research Letters, 14, 035 001, https://doi.org/10.1088/1748-9326/aaf34b, 2019.

Glooschenko, W., Tarnocai, C., Zoltai, S., and Glooschenko, V.: Wetlands of Canada and Greenland, in: Wetlands of the world: inventory, ecology and management, chap. Wetlands of Canada and Greenland, pp. 415–514, Kluwer Academic Publishers, Dordrecht, The Netherlands, handbook of vegetation science 15/2 edn., https://doi.org/-, 1993.

Gorham, E.: Northern Peatlands: Role in the Carbon Cycle and Probable Responses to Climatic Warming, Ecological Applications, 1, 182–195, http://www.jstor.org/stable/1941811, 1991.

Harenda, K., Lamentowicz, M., Samson, M., and Chojnicki, B.: The Role of Peatlands and Their Carbon Storage Function in the Context of Climate Change, pp. 169–187, Springer International Publishing, https://doi.org/10.1007/978-3-319-71788-3_12, 2018.

Horwath Burnham, J. and Sletten, R.: Spatial distribution of soil organic carbon in northwest Greenland and underestimates of High Arctic carbon stores, Global Biogeochemical Cycles, 24, https://doi.org/10.1029/2010gb003933, 2010.

Hossain, M., Chen, W., and Zhang, Y.: Bulk density of mineral and organic soils in the Canada's arctic and sub-arctic, Information Processing in Agriculture, 2, 183 – 190, https://doi.org/https://doi.org/10.1016/j.inpa.2015.09.001, 2015.

5 Hugelius, G., Tarnocai, C., Broll, G., Canadell, J. G., Kuhry, P., and Swanson, D. K.: The northern circumpolar soil carbon database: Spatially distributed datasets of soil coverage and soil carbon storage in the northern permafrost regions, Earth System Science Data, 5, 3–13, https://doi.org/10.5194/essd-5-3-2013, 2013.

Jammet, M., Dengel, S., Kettner, E., Parmentier, F.-J. W., Wik, M., Crill, P., and Friborg, T.: Year-round CH_4 and CO_2 flux dynamics in two contrasting freshwater ecosystems of the subarctic, Biogeosciences, 14, 5189–5216, https://doi.org/10.5194/bg-14-5189-2017, 2017.

10 Jungkunst, H. F., Krüger, J. P., Heitkamp, F., Erasmi, S., Fiedler, S., Glatzel, S., and Lal, R.: Accounting More Precisely for Peat and Other Soil Carbon Resources, pp. 127–157, Springer Netherlands, Dordrecht, https://doi.org/10.1007/978-94-007-4159-1_7, 2012.

Karami, M., Westergaard-Nielsen, A., Normand, S., Treier, U. A., Elberling, B., and Hansen, B. U.: A phenology-based approach to the classification of Arctic tundra ecosystems in Greenland, ISPRS Journal of Photogrammetry and Remote Sensing, 146, 518 – 529, https://doi.org/https://doi.org/10.1016/j.isprsjprs.2018.11.005, 2018.

15 Kicklighter, D., Melillo, J., Monier, E., Sokolov, A., and Zhuang, Q.: Future nitrogen availability and its effect on carbon sequestration in Northern Eurasia, Nature Communications, 10, https://doi.org/10.1038/s41467-019-10944-0, 2019.

Krüger, J. P., Leifeld, J., Glatzel, S., Szidat, S., and Alewell, C.: Biogeochemical indicators of peatland degradation – a case study of a temperate bog in northern Germany, Biogeosciences, 12, 2861–2871, https://doi.org/10.5194/bg-12-2861-2015, 2015.

Kuhry, P. and Vitt, D.: Fossil Carbon/Nitrogen Ratios as a Measure of Peat Decomposition, Ecology, 77, 271,
20 https://doi.org/10.2307/2265676, 1996.

Largeron, C., Krinner, G., Ciais, P., and Brutel-Vuilmet, C.: Implementing northern peatlands in a global land surface model: Description and evaluation in the ORCHIDEE high-latitude version model (ORC-HL-PEAT), Geoscientific Model Development, 11, 3279–3297, https://doi.org/10.5194/gmd-11-3279-2018, 2018.

Larsen, N. K., Strunk, A., Levy, L. B., Olsen, J., Bjørk, A., Lauridsen, T. L., Jeppesen, E., and Davidson, T. A.: Strong altitudinal con-
25 trol on the response of local glaciers to Holocene climate change in southwest Greenland, Quaternary Science Reviews, 168, 69 – 78, https://doi.org/https://doi.org/10.1016/j.quascirev.2017.05.008, 2017.

Leifeld, J. and Menichetti, L.: The underappreciated potential of peatlands in global climate change mitigation strategies, Nature Communications, 9, https://doi.org/10.1038/s41467-018-03406-6, 2018.

Limpens, J., Berendse, F., Blodau, C., Canadell, J. G., Freeman, C., Holden, J., Roulet, N., Rydin, H., and Schaepman-Strub, G.: Peatlands
30 and the carbon cycle: from local processes to global implications – a synthesis, Biogeosciences, 5, 1475–1491, https://doi.org/10.5194/bg-5-1475-2008, https://www.biogeosciences.net/5/1475/2008/, 2008.

Loisel, J., Yu, Z., Beilman, D., Camill, P., Alm, J., J Amesbury, M., Anderson, D., Andersson, S., Bochicchio, C., Barber, K., Belyea, L., Bunbury, J., Chambers, F., Charman, D., Vleeschouwer, F., Fiałkiewicz-kozieł, B., Finkelstein, S., Gałka, M., Garneau, M., and Zhou, W.: A database and synthesis of northern peatland soil properties and Holocene carbon and nitrogen accumulation, The Holocene, 24,
35 https://doi.org/10.1177/0959683614538073, 2014.

Luan, J., Wu, J., Liu, S., Roulet, N., and Wang, M.: Soil nitrogen determines greenhouse gas emissions from northern peatlands under concurrent warming and vegetation shifting, Communications Biology, 2, https://doi.org/10.1038/s42003-019-0370-1, 2019.

Lüers, J., Westermann, S., Piel, K., and Boike, J.: Annual CO_2 budget and seasonal CO_2 exchange signals at a high Arctic permafrost site on Spitsbergen, Svalbard archipelago, Biogeosciences, 11, 6307–6322, https://doi.org/10.5194/bg-11-6307-2014, 2014.

MacDonald, G. M., Beilman, D. W., Kremenetski, K. V., Sheng, Y., Smith, L. C., and Velichko, A. A.: Rapid Early Development of Circum-arctic Peatlands and Atmospheric CH4 and CO2 Variations, Science, 314, 285–288, https://doi.org/10.1126/science.1131722, 2006.

5 Michaelson, G., Ping, C.-L., and Clark, M.: Soil Pedon Carbon and Nitrogen Data for Alaska: An Analysis and Update, Open Journal of Soil Science, 03, 132–142, https://doi.org/10.4236/ojss.2013.32015, 2013.

Morel, X., Decharme, B., Delire, C., Krinner, G., Lund, M., Hansen, B. U., and Mastepanov, M.: A New Process-Based Soil Methane Scheme: Evaluation Over Arctic Field Sites With the ISBA Land Surface Model, Journal of Advances in Modeling Earth Systems, 0, https://doi.org/10.1029/2018MS001329, 2019a.

10 Morel, X., Hansen, B. U., Delire, C., Ambus, P. L., Mastepanov, M., and Decharme, B.: Soil Carbon and Nitrogen stocks and profiles from an instrumented Greenlandic fen, https://doi.org/10.1594/PANGAEA.909899, 2019b.

Noilhan, J. and Planton, S.: A Simple Parameterization of Land Surface Processes for Meteorological Models, Monthly Weather Review, 117, 536–549, https://doi.org/10.1175/1520-0493(1989)117<0536:ASPOLS>2.0.CO;2, 1989.

Palmtag, J., Hugelius, G., Lashchinskiy, N., Tamstorf, M. P., Richter, A., Elberling, B., and Kuhry, P.: Storage, landscape distribution, and
15 burial history of soil organic matter in contrasting areas of continuous permafrost, Arctic, Antarctic, and Alpine Research, 47, 71–88, https://doi.org/10.1657/aaar0014-027, 2015.

Palmtag, J., Cable, S., Christiansen, H. H., Hugelius, G., and Kuhry, P.: Landform partitioning and estimates of deep storage of soil organic matter in Zackenberg, Greenland, The Cryosphere, 12, 1735–1744, https://doi.org/10.5194/tc-12-1735-2018, 2018.

Pastukhov, A. and Kaverin, D.: Soil carbon pools in tundra and taiga ecosystems of northeastern Europe, Eurasian Soil Science, 46, 958–967,
20 https://doi.org/10.1134/S1064229313070077, 2013.

Ping, C.-L., Michaelson, G. J., Guo, L., Jorgenson, M. T., Kanevskiy, M., Shur, Y., Dou, F., and Liang, J.: Soil carbon and material fluxes across the eroding Alaska Beaufort Sea coastline, Journal of Geophysical Research: Biogeosciences, 116, https://doi.org/10.1029/2010JG001588, 2011.

Pirk, N., Tamstorf, M. P., Lund, M., Mastepanov, M., Pedersen, S. H., Mylius, M. R., Parmentier, F. J. W., Christiansen, H. H., and Chris-
25 tensen, T. R.: Snowpack fluxes of methane and carbon dioxide from high Arctic tundra, Journal of Geophysical Research: Biogeosciences, 121, 2886–2900, https://doi.org/10.1002/2016JG003486, 2016.

Pirk, N., Mastepanov, M., López-Blanco, E., Christensen, L. H., Christiansen, H. H., Hansen, B. U., Lund, M., Parmentier, F. J. W., Skov, K., and Christensen, T. R.: Toward a statistical description of methane emissions from arctic wetlands, Ambio, 46, 70–80, https://doi.org/10.1007/s13280-016-0893-3, 2017.

30 Qiu, C., Zhu, D., Ciais, P., Guenet, B., Krinner, G., Peng, S., Aurela, M., Bernhofer, C., Brümmer, C., Bret-Harte, S., Chu, H., Chen, J., Desai, A. R., Dušek, J., Euskirchen, E. S., Fortuniak, K., Flanagan, L. B., Friborg, T., Grygoruk, M., Gogo, S., Grünwald, T., Hansen, B. U., Holl, D., Humphreys, E., Hurkuck, M., Kiely, G., Klatt, J., Kutzbach, L., Largeron, C., Laggoun-Défarge, F., Lund, M., Lafleur, P. M., Li, X., Mammarella, I., Merbold, L., Nilsson, M. B., Olejnik, J., Ottosson-Löfvenius, M., Oechel, W., Parmentier, F.-J. W., Peichl, M., Pirk, N., Peltola, O., Pawlak, W., Rasse, D., Rinne, J., Shaver, G., Schmid, H. P., Sottocornola, M., Steinbrecher, R., Sachs, T., Urbaniak, M.,
35 Zona, D., and Ziemblinska, K.: ORCHIDEE-PEAT (revision 4596), a model for northern peatland CO_2, water, and energy fluxes on daily to annual scales, Geoscientific Model Development, 11, 497–519, https://doi.org/10.5194/gmd-11-497-2018, 2018.

Quinton, W., Gray, D., and Marsh, P.: Subsurface drainage from hummock-covered hillslopes in the Arctic tundra, Journal of Hydrology, 237, 113–125, https://doi.org/10.1016/S0022-1694(00)00304-8, 2000.

Raich, J. W. and Schlesinger, W. H.: The global carbon dioxide flux in soil respiration and its relationship to vegetation and climate, Tellus B, 44, 81–99, https://doi.org/10.1034/j.1600-0889.1992.t01-1-00001.x, 1992.

Raundrup, K., Aastrup, P., Nyman, J., Lauridsen, T. L., Sander Johannsson, L., Henning Krogh, P., Lund, M., and Rasmussen, L. M.: NUUK BASIC: The BioBasis programme, in: Nuuk Ecological Research Operations, 3rd Annual Report, 2009, edited by Jensen, L. and Rasch, M., National Environmental Research Institute, Aarhus University, 2010.

Rezanezhad, F., S. Price, J., L. Quinton, W., Lennartz, B., Milojevic, T., and Van Cappellen, P.: Structure of peat soils and implications for water storage, flow and solute transport: A review update for geochemists, Chemical Geology, 429, https://doi.org/10.1016/j.chemgeo.2016.03.010, 2016.

Rößger, N., Wille, C., Holl, D., Göckede, M., and Kutzbach, L.: Scaling and balancing carbon dioxide fluxes in a heterogeneous tundra ecosystem of the Lena River Delta, Biogeosciences, 16, 2591–2615, https://doi.org/10.5194/bg-16-2591-2019, https://www.biogeosciences.net/16/2591/2019/, 2019.

Rydin, H. and Jeglum, J.: The biology of peatlands, second edition., Oxford University Press, 2013.

Sachs, T., Wille, C., Boike, J., and Kutzbach, L.: Environmental controls on ecosystem-scale CH$_4$ emission from polygonal tundra in the Lena River Delta, Siberia, Journal of Geophysical Research, 113, G00A03, https://doi.org/10.1029/2007JG000505, 2008.

Schlesinger, W. H. and Bernhardt, E. S.: Wetland Ecosystems, in: Biogeochemistry, chap. Wetland ecosystems, pp. 233–274, Academic Press, Oxford, UK, elsevier edn., https://doi.org/10.1016/B978-0-12-385874-0.00007-8, 2013.

Siewert, M., Hanisch, J., Weiss, N., Kuhry, P., C. Maximov, T., and Hugelius, G.: Comparing carbon storage of Siberian tundra and taiga permafrost ecosystems at very high spatial resolution, Journal of Geophysical Research: Biogeosciences, 120, 1973 – 1994, https://doi.org/10.1002/2015JG002999, 2015.

Siewert, M., Hugelius, G., Heim, B., and Faucherre, S.: Landscape controls and vertical variability of soil organic carbon storage in permafrost-affected soils of the Lena River Delta, Catena, 147, 725 – 741, https://doi.org/10.1016/j.catena.2016.07.048, 2016.

Sigsgaard, C., Thorsøe, K., Fugl, A., Mastepanov, M., Friborg, T., Tamstorf, M., Hansen, B., Ström, L., and Røjle Christensen, T.: Zackenberg Basic: The Climate Basis and GeoBasis programmes, in: 12th Annual Report 2006, Zackenberg Ecological Research Operations, National Environmental Research Institute, Aarhus University, 2007.

Tamstorf, M., Iversen, K., Hansen, B., Sigsgaard, C., Fruergaard, M., Andreasen, R., Mastepanov, M., Falk, J., Ström, L., and Christensen, T.: NUUK BASIC: The GeoBasis programme, in: Nuuk Ecological Research Operations, 1st Annual Report, 2007, edited by Jensen, L. and Rasch, M., National Environmental Research Institute, Aarhus University, 2008.

van der Molen, M. K., van Huissteden, J., Parmentier, F. J. W., Petrescu, A. M. R., Dolman, A. J., Maximov, T. C., Kononov, A. V., Karsanaev, S. V., and Suzdalov, D. A.: The growing season greenhouse gas balance of a continental tundra site in the Indigirka lowlands, NE Siberia, Biogeosciences, 4, 985–1003, https://doi.org/10.5194/bg-4-985-2007, 2007.

Vitousek, P. and Howarth, R.: Nitrogen limitation on land and in the sea: how can it occur? Biogeochemistry 13:87-115, Biogeochemistry, 13, 87–115, https://doi.org/10.1007/BF00002772, 1991.

Voigt, C., Marushchak, M. E., Lamprecht, R. E., Jackowicz-Korczyński, M., Lindgren, A., Mastepanov, M., Granlund, L., Christensen, T. R., Tahvanainen, T., Martikainen, P. J., and Biasi, C.: Increased nitrous oxide emissions from Arctic peatlands after permafrost thaw, Proceedings of the National Academy of Sciences, 114, 6238–6243, https://doi.org/10.1073/pnas.1702902114, https://www.pnas.org/content/114/24/6238, 2017.

Wang, M., Moore, T. R., Talbot, J., and Riley, J. L.: The stoichiometry of carbon and nutrients in peat formation, Global Biogeochemical Cycles, 29, 113–121, https://doi.org/10.1002/2014GB005000, 2015.

Xu, J., Morris, P. J., Liu, J., and Holden, J.: PEATMAP: Refining estimates of global peatland distribution based on a meta-analysis, CATENA, 160, 134 – 140, https://doi.org/https://doi.org/10.1016/j.catena.2017.09.010, http://www.sciencedirect.com/science/article/pii/S0341816217303004, 2018.

Yu, Z., Loisel, J., Brosseau, D. P., Beilman, D. W., and Hunt, S. J.: Global peatland dynamics since the Last Glacial Maximum, Geophysical Research Letters, 37, https://doi.org/10.1029/2010GL043584, 2010.

Yu, Z., Beilman, D. W., Frolking, S., MacDonald, G. M., Roulet, N. T., Camill, P., and Charman, D. J.: Peatlands and Their Role in the Global Carbon Cycle, Eos, Transactions American Geophysical Union, 92, 97–98, https://doi.org/10.1029/2011EO120001, 2011.

Yu, Z. C.: Northern peatland carbon stocks and dynamics: a review, Biogeosciences, 9, 4071–4085, https://doi.org/10.5194/bg-9-4071-2012, 2012.

5

Table 1. Short review of available carbon stocks, profiles, CO_2 and CH_4 fluxes for different sites

Site	C stock (<1m)	C profile	CO_2 [1]	CH_4 [1]	loc(C) = loc(GHG) [2]	Reference
Abisko	Yes[3]	Yes[4]	ET	ET	No	Jammet et al. (2017); Chadburn et al. (2017)
Bayelva	Yes[3]	Yes[4]	ET	No	No	Lüers et al. (2014); Chadburn et al. (2017)
Kytalyk	Yes[3]	Yes[4]	ET ; MC	MC	No	van der Molen et al. (2007); Chadburn et al. (2017)
Samoylov	Yes[3]	Yes[4]	ET	ET	No	Sachs et al. (2008); Siewert et al. (2015, 2016); Rößger et al. (2019)
Zackenberg	Yes[3]	Yes[4]	ET ; AC	AC	No	Pirk et al. (2016, 2017); Chadburn et al. (2017); Sigsgaard et al. (2007)
Seida	Yes	No	ET	ET	NA	Pastukhov and Kaverin (2013)
Adventdalen	No	No	AC	AC	NA	Pirk et al. (2016, 2017)
Nuuk	This study	This study	ET ; AC	AC	Yes	Pirk et al. (2016, 2017); Tamstorf et al. (2008); Raundrup et al. (2010)

(1) ET : Eddy Tower ; MC : Manual Chambers ; AC : Automatic Chambers

(2) loc(C) : Localisation of soil carbon data measurement ; loc(GHG) localisation of greenhouse gas fluxes measurement. NA = Not Announced

(3) computed via combination and harmonization of several plots (Palmtag et al., 2015; Siewert et al., 2015, 2016)

(4) computed via weighted average (Palmtag et al., 2015; Siewert et al., 2015, 2016)

Table 2. Data statistics and dispersion (mean, median, lower and upper decile)

	mean	median	lower decile	upper decile
soil sample density ρ_{sample} (g.cm^{-3})	0.940	0.898	0.445	1.528
soil bulk density ρ_{bulk}^{obs} (g.cm^{-3})	0.345	0.187	0.065	0.978
soil water content f_{wet} (%)	69.5	79.0	29.8	86.9
C/N Ratio (-)	21.6	21.0	17.1	25.9
soil carbon content f_C (%)	27.0	31.5	3.1	44.1
soil carbon density ρ_C (kgC.m^{-3})	50.2	44.8	13.1	93.3
soil nitrogen content f_N (%)	1.27	1.37	0.44	2.12
soil nitrogen density ρ_N (kgN.m^{-3})	2.37	2.25	0.59	4.17

Table 3. Carbon and nitrogen stocks from peat cores along the first transect

Peat core of transect 1 (m)	0	5	10	15	20	25	30	35	Mean	Std
Maximum sampling depth (cm)	55	75	65	85	95	85	75	75	76.3	12.5
Number of samples (-)	7	8	7	9	10	8	8	7	8	-
C_T (kgC.m^{-2})	31.8	58.9	37.2	29.2	46.7	55.4	40.5	34.5	41.8	10.9
N_T (kgN.m^{-2})	1.7	2.9	1.6	1.4	2.2	2.4	1.9	1.7	2.0	0.5

Table 4. Carbon and nitrogen stocks from peat cores along the second transect

Peat core of transect 2 (m)	0	10	20	30	40	50	60	70	80	Mean	Std
Maximum sampling depth (cm)	85	85	85	95	65	65	65	45	70	73.3	15.4
Number of samples (-)	8	9	10	11	7	7	7	5	7	7.8	-
C_T (kgC.m^{-2})	35.4	38.4	53.4	39.1	22.2	21.6	27.3	16.6	28.6	31.4	11.3
N_T (kgN.m^{-2})	1.6	1.8	2.3	2.0	1.0	1.0	1.5	0.8	1.4	1.5	0.5

**Table 5.** Statistical scores for different regressions between bulk density ρ_{bulk} and carbon content f_C

Regression type		$r^{2\,(1)}$	c-rmse$^{(2)}$	mae$^{(3)}$	bias$^{(4)}$
Hossain et al. (2015)	$\rho_{bulk}^{H} = 1.5641 \times e^{-0.0631 f_C}$	0.801	0.196	0.154	-0.10
Exponential	$\rho_{bulk}^{exp} = 0.7276 \times e^{-0.04583 f_C}$	0.760	0.222	0.147	0.07
Power	$\rho_{bulk}^{pow} = 1.8975 \times f_C^{-0.73794}$	0.817	0.164	0.117	0.032
Logarithmic	$\rho_{bulk}^{log} = -0.3281 \times \ln(f_C) + 1.31736$	0.832	0.152	0.114	- 10^{-4}

(1) $r^2 = \left(\dfrac{\sum_{i=1}^{n} (x_i - \overline{y})(f(x_i) - \overline{f})}{\sqrt{\sum_{i=1}^{n} (x_i - \overline{x})^2} \sqrt{\sum_{i=1}^{n} (f_i - \overline{f})^2}} \right)^2$

(2) c-rmse $= \dfrac{1}{n} \sqrt{\sum \left(x_i - \overline{x} - (f(x_i) - \overline{f}) \right)^2}$

(3) mae $= \dfrac{1}{n} \sum_{i=1}^{n} |x_i - f(x_i)|$

(4) bias $= \dfrac{1}{n} \sum_{i=1}^{n} (x_i - f(x_i))$
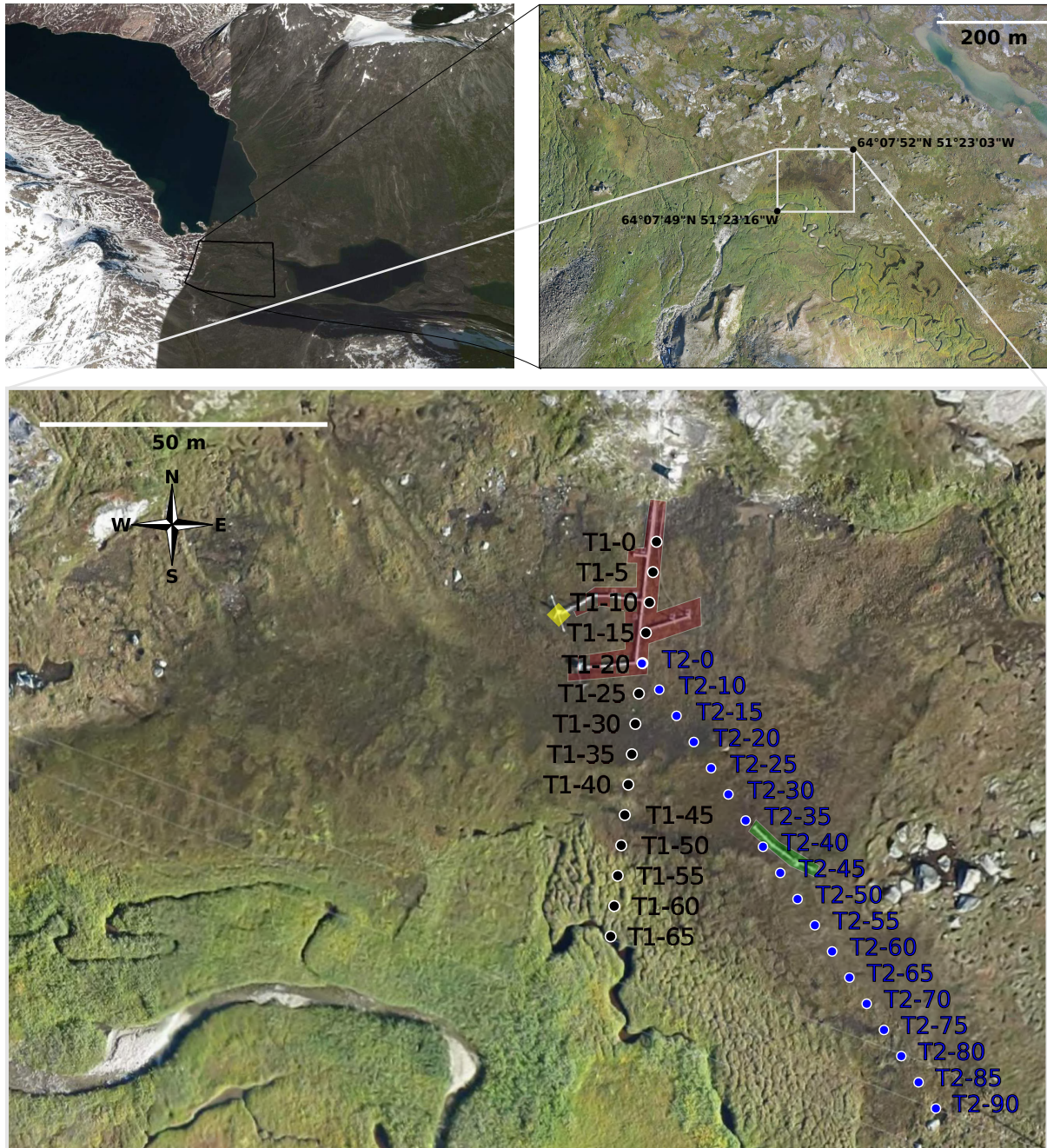
Figure 1. Left-top panel : satelite image (Google Earth© - 2009) of Kobbefjord, centered on 64°7'51.5"N ; 51°23'10.5"W. Right-top panel : high-resolution photography (taken by a drone in 2015) of the valley floor. The white rectangle surrounds the fen. Bottom-panel : zoom of the fen, with the two studied transects : T1 (black circles) and T2 (blue circles). Zones highlighted in red represent the location of the automatic chambers ; in green, the soil temperature probes ; in yellow, the eddy flux tower.

23
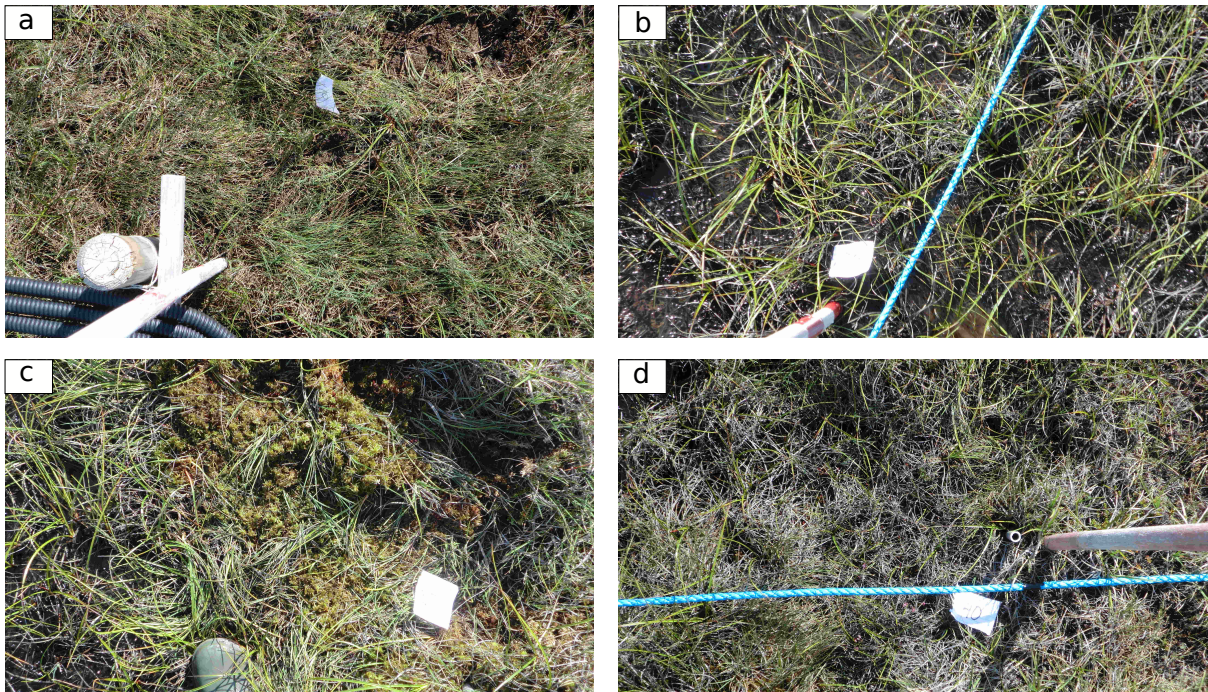
Figure 2. Soil surface photographs along the first transect at several plots. **(a)** : T1-10 ; **(b)** : T1-30 ; **(c)** : T1-35 ; **(d)** : T1-40.
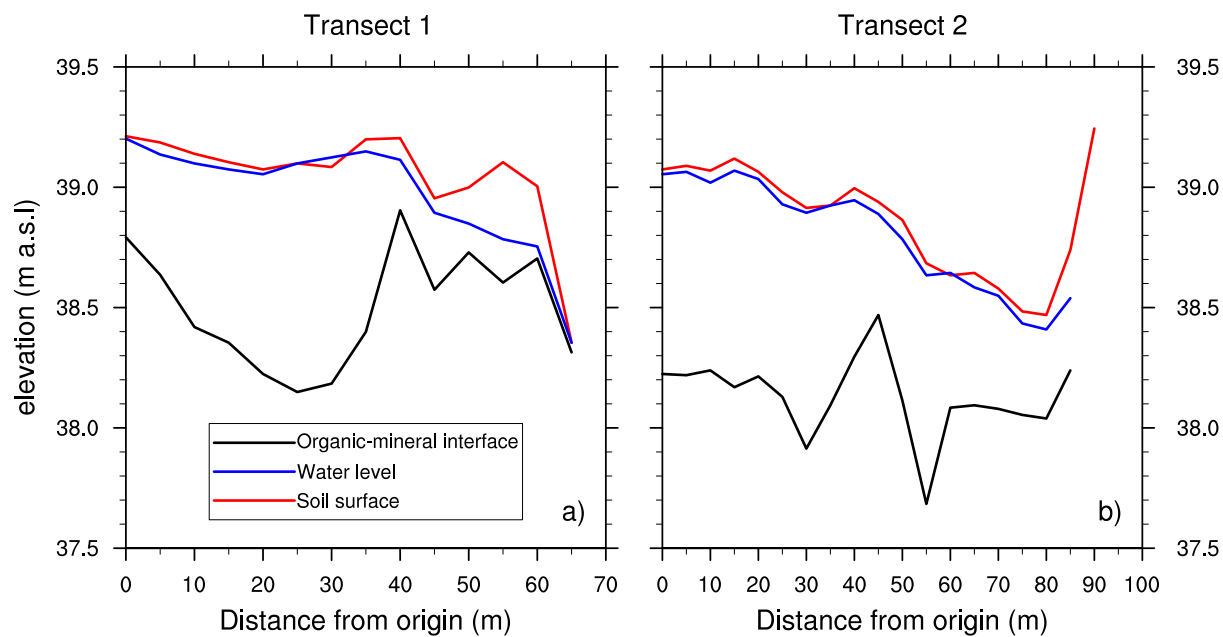
Figure 3. Topographical measurements of soil surface (red) and manual measurements of water level (blue) and organic-mineral interface (black) along both transects. Manual measurements of water level were made in July, 27th 2017.

Figure 4. First transect soil samples after 48 hours of oven drying at 80 °C. Different samples depths are shown for plots **(a)** : $T1-10$; **(b)** : $T1-25$.
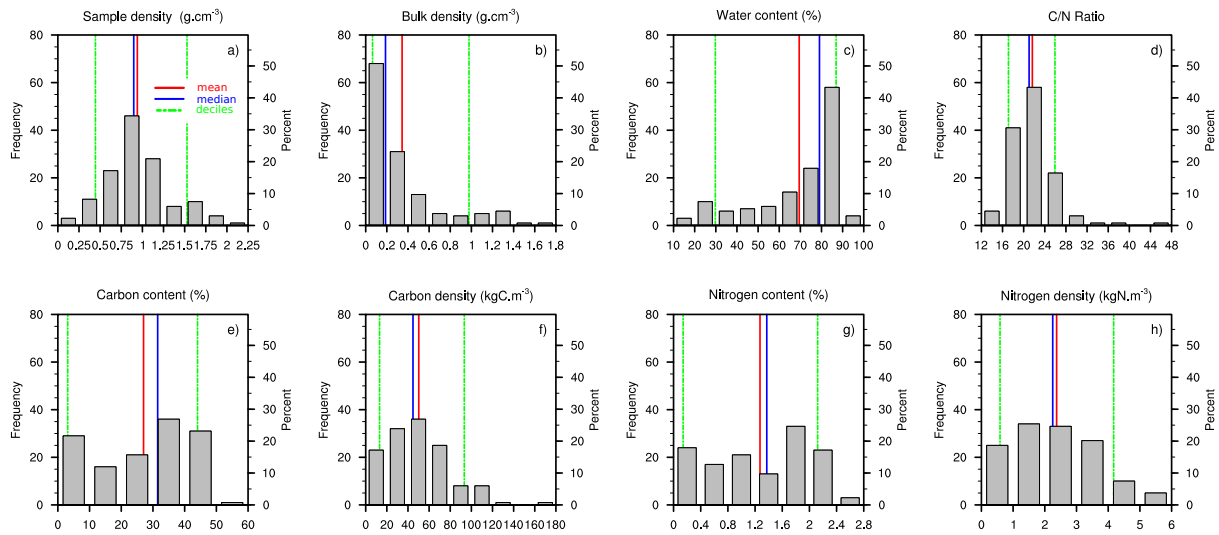
Figure 5. Distribution histograms ($n_{samples} = 135$) of **(a)** soil sample density ρ_{sample} (g.cm^{-3}) ; **(b)** soil bulk density ρ_{bulk}^{obs} (g.cm^{-3}) ; **(c)** soil water content (%) ; **(d)** C/N Ratio (-) ; **(e)** soil carbon content f_C (%) ; **(f)** soil carbon density ρ_C (kgC.m^{-3}) ; **(g)** soil nitrogen content f_N (%) ; **(h)** soil nitrogen density ρ_N (kgN.m^{-3}). Red lines represent mean values , blue lines median values , dashed green lines upper and lower deciles.
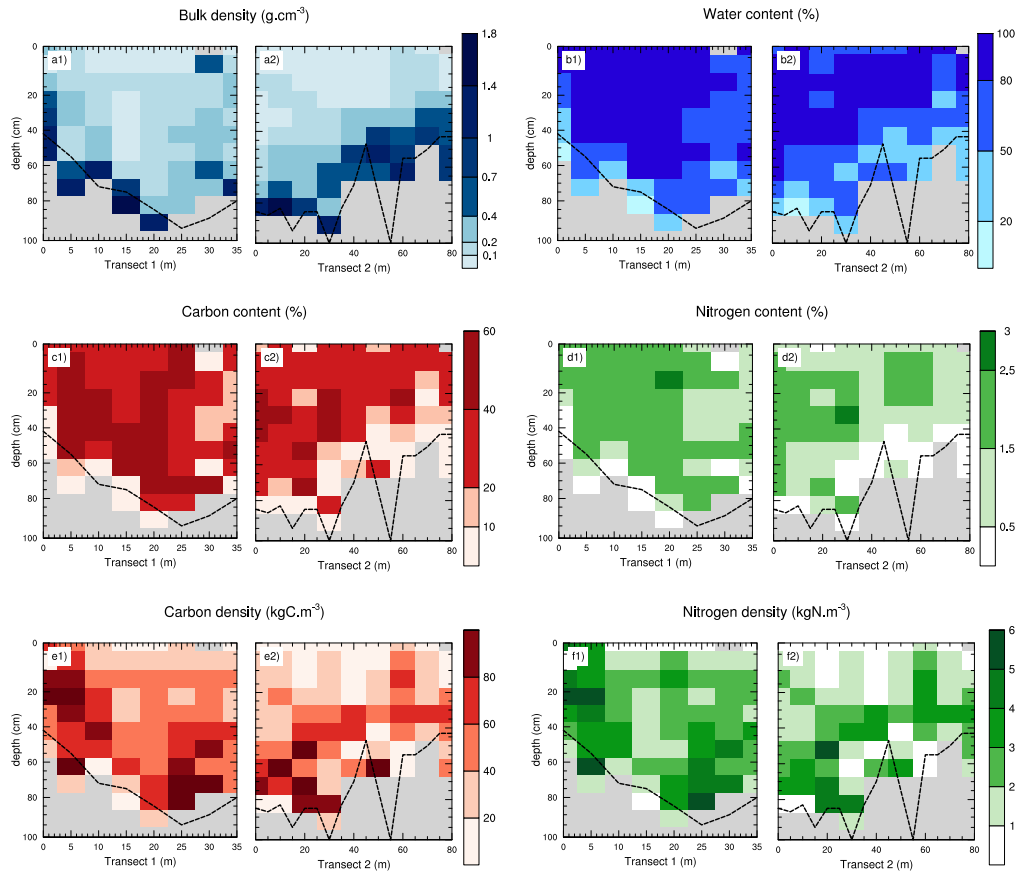
Figure 6. Soil profiles of **(a)** soil bulk density ρ_{bulk}^{obs} (g.cm^{-3}) ; **(b)** soil water content (%) ; **(c)** soil carbon content f_C (%) ; **(d)** soil nitrogen content f_N (%) ; **(e)** soil carbon density ρ_C (kgC.m^{-3}) ; **(f)** soil nitrogen density ρ_N (kgN.m^{-3}) along both transects. Dashed black line represents the measured organic-mineral interface. Grey zones indicates the absence of data (mineral soil).
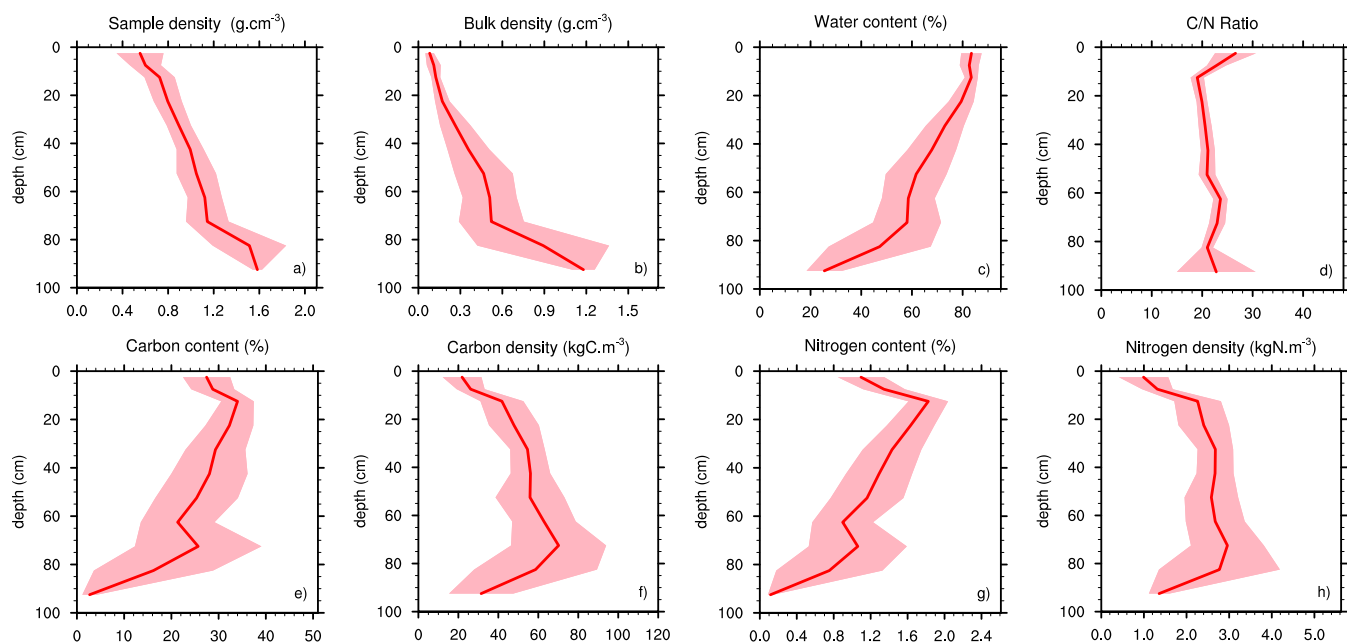
Figure 7. Mean soil profiles over both transects ($n_{samples} = 135$; $n_{profiles} = 17$) of **(a)** soil sample density ρ_{sample} (g.cm^{-3}) ; **(b)** soil bulk density ρ_{bulk}^{obs} (g.cm^{-3}) ; **(c)** soil water content (%) ; **(d)** C/N Ratio (-) ; **(e)** soil carbon content f_C (%) ; **(f)** soil carbon density ρ_C (kgC.m^{-3}) ; **(g)** soil nitrogen content f_N (%) ; **(h)** soil nitrogen density ρ_N (kgN.m^{-3}). Shaded area represents the 95% confidence interval.
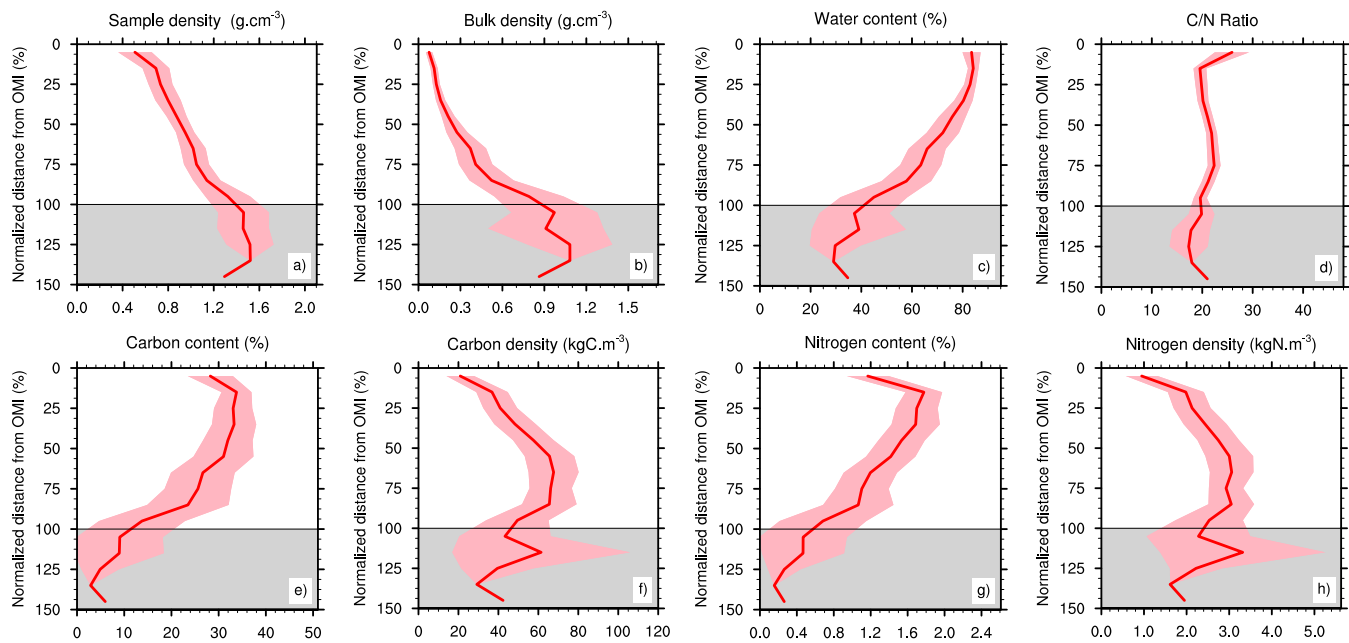
Figure 8. Same than figure 7, except profiles depth are re-normalized from organic-mineral interface. Grey area represents the zone below the OMI.
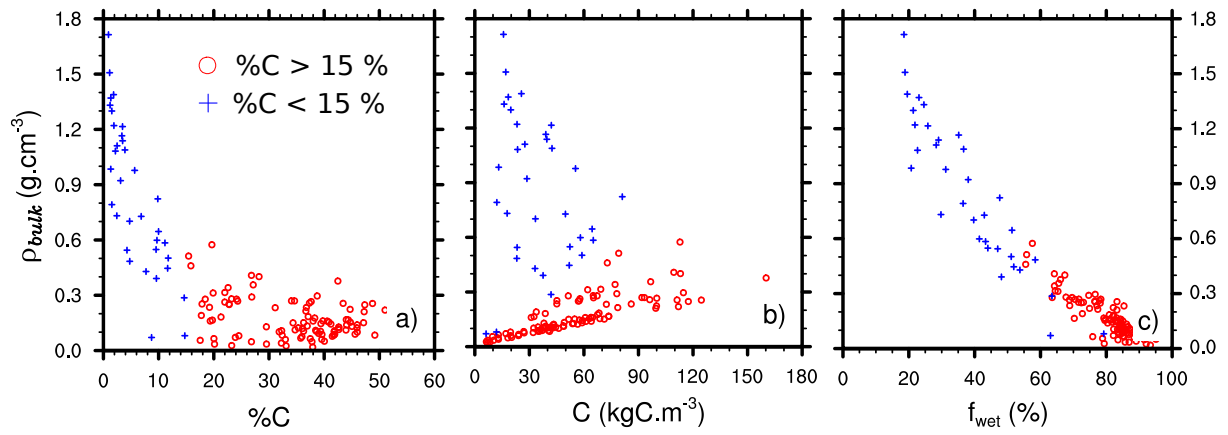
Figure 9. Scatter plots of soil bulk density ρ_{bulk}^{obs} versus **(a)** soil carbon content f_C (%) ; **(b)** soil carbon density ρ_C (kgC.m^{-3}) ; **(c)** soil water content (%) for the 135 samples. Red circles represents samples with carbon content exceeding 15 %, blue crosses less than 15 %.